Eur. Phys. J. Plus (2024) 139:857
https://doi.org/10.1140/epjp/s13360-024-05631-z

THE EUROPEAN PHYSICAL JOURNAL PLUS

Regular Article

Effect of perfect fluid dark matter on Bardeen thin-shell wormholes

Asifa Ashraf[1,a], **Faisal Javed**[2,3,b], **Wen-Xiu Ma**[1,4,5,6,c], **Arfa Waseem**[7,d]

[1] School of Mathematical Sciences, Zhejiang Normal University, Jinhua 321004, Zhejiang, China
[2] Department of Physics, Zhejiang Normal University, Jinhua 321004, People's Republic of China
[3] National Research University TIIAME, Kori Niyoziy 39, Tashkent 100000, Uzbekistan
[4] Department of Mathematics, King Abdulaziz University, 21589 Jeddah, Saudi Arabia
[5] Department of Mathematics and Statistics, University of South Florida, Tampa, FL 33620-5700, USA
[6] School of Mathematical and Statistical Sciences, North-West University, Mafikeng Campus, Private Bag X2046, Mmabatho 2735, South Africa
[7] Department of Mathematics, Government College Women University, Sialkot, Pakistan

Received: 15 January 2024 / Accepted: 29 August 2024
© The Author(s), under exclusive licence to Società Italiana di Fisica and Springer-Verlag GmbH Germany, part of Springer Nature 2024

Abstract In the context of perfect fluid dark matter, this study examines the formation and stability of Bardeen thin-shell wormholes. The mathematical structure of equivalent copies of Bardeen black holes with perfect fluid dark matter is used to create the thin-shell wormholes via cut-and-paste method. Utilizing linearized radial perturbation analysis, the study's main objective is to explore the stable geometry of these wormholes. We study the effect of variable equations of state on the stability of the wormholes, including barotropic, variable Chaplygin, and phantom-like equations of states. The investigation emphasizes the inclusion of dark matter, an unsolved mystery part that makes up a sizeable amount of the universe's mass, and explores how various equations of state for the dark matter affect the stability and characteristics of the wormholes. The discoveries improved our comprehension of both phenomena and their possible implications for further space travel by shedding insight on the interactions between wormholes and dark matter.

1 Introduction

Black holes (BHs) are considered as the most enigmatic as well as complex celestial objects due to their singularities surrounded by the event horizons. A singularity in the field of general relativity (GR) is such an era of spacetime where all physical rules fail to apply and gravitational pull diverges there. The occurrence of such region is one of the fundamental issues of the theory of GR. A system of solutions known as "regular BHs" have been crucial in avoiding these undefinable regions because they do not contain such singularity at their origin. The first ever solution of the spherically symmetric regular BH was determined by Bardeen [1], recognized as the Bardeen BH. Later on, following the notion of Bardeen BH, few more regular BHs were proposed in literature [2–4]. Cataldo and García [5] derived the solutions of (2+1)-dimensional regular BH under the influence of a nonlinear electric field. Dymnikova [6] exhibited the presence of the spherically symmetric charged regular solutions of the BH with nonlinear electrodynamics. Hayward [7] described the formation as well as evaporation of the regular BHs and discussed their distinct regions. In the light of GR, some other features of such regular BHs have also been studied by employing different techniques [8, 9].

Currently, one of the most fascinating research in GR is the study of wormhole (WH) structures as well as their solutions, which has intrigued several researchers. According to GR, the existence of such mysterious geometries is feasible due to the deformable spacetime carried out by matter or energy. Actually, the WHs act as the bridges for two different places at a manifold. The WHs possess asymptotically flat geometry, and this concept was first presented by Flamm [10]. After that, Einstein and Rosen [11] proposed the WH geometry known as "Einstein–Rosen bridge" which is also characterized as the vacuum solution of Einstein's field equations. These WH structures are formulated by joining two BHs as two different eras of spacetime. It is predicted that such WHs are not traversable due the occurrence of singularity. The geometry of Schwarzschild WH being the non-traversable structure is described by Fuller and Wheeler [12] with the help of Kruskal constituents. In order to explore the existence of WHs having traversable nature, numerous researchers considered the theoretical observations from Schwarzschild WH as well as the Einstein–Rosen bridges.

[a] e-mail: asifamustafa3828@gmail.com
[b] e-mail: faisaljaved.math@gmail.com
[c] e-mail: wma3@usf.edu (corresponding author)
[d] e-mail: arfa.waseem@gcwus.edu.pk (corresponding author)

Published online: 26 September 2024

Blazquez-Salcedo [13] presented a concrete instance of a category of traversable wormholes in the context of Einstein–Dirac—Maxwell theory in four-dimensional spacetime. Remarkably, these wormholes do not require any form of unconventional matter [13]. By considering a scenario involving two massive fermions in a singlet spinor state, they demonstrated the presence of spherically symmetric asymptotically flat structures that are devoid of singularities. These configurations represent localized states. Furthermore, these solutions adhere to a generalized Smarr relation and exhibit a connection with extremal Reissner–Nordström black holes [13]. Konoplya and Zhidenko [14] demonstrated the existence of wormhole solutions that exhibit asymmetry with respect to the throat and possess smooth gravitational and matter fields, hence avoiding all the aforementioned issues. This suggests that such wormhole structures might possibly be sustained in a plausible scenario [14]. Wang et al. [15] pointed out that a physically relevant condition on the throat is imposed to lead to no gravitational force experienced by a stationary observer at the throat is not necessary.

The primary traversable WH configuration is demonstrated by Morris and Thorne [16] that connects the different cosmic domains or two distant cosmos through a throat that makes it possible to travel across different spacetime eras. It is also observed that to pass across this throat, the matter content inside this geometry must disobey the usual energy bounds [16–19]. So, according to GR, the inclusion of exotic matter violating the energy bounds is the necessary ingredient for the occurrence of such WH geometry. This problem was solved by the development of thin-shell WHs, where the amount of exotic matter may be limited to the necessary minimum amount that disobey the energy bound only in this region [20, 21]. Such WH structure is made possible by taking into account the well-known cut-and-paste strategy where cutting and pasting is applied at different manifolds to generate a new structure possessing a shell at the joining region. During this procedure, the required amount of exotic component is engrossed in the WH throat. As, one cannot ignore it, therefore, researchers prefer the thin-shell structure of WHs. At the WH throat, the surface-energy tensor contents can be determined via Darmois–Israel condition [22, 23] that further yields the Lanczos equations [24–26]. The dynamic conversion in the geometry of WH can be observed by finding the solution of the Lanczos equation corresponding to the equation of state (EoS) for the exotic component on the thin shell.

The stability analysis assists in the exploration of numerous universe-wide WH geometries that can be studied either through the use of radial perturbations or by considering the existence of an EoS for the exotic content inside the WH throat. The structures of traversable WHs are of great importance if they exhibit stable geometry against linear perturbations. In this respect, several authors inspected the WH stable structures along with the thin-shell WHs by utilizing the linear perturbations to preserve the real symmetries. The stable geometry of Schwarzschild thin-shell WH has been inspected by Poisson and Visser [27]. With the inclusion of cosmological constant, Lobo and Crawford [28] examined the stable configuration of thin-shell WHs and observed that the viable solutions appear only for the positive choices of the cosmological constant. Eiroa and Romero [29] determined the stable WH solutions under the effect of electric field and exhibited that WHs possess stable geometries just for some particular choices of the charge factor. The stable geometry of thin-shell WH along with the regular BH for a phantom scalar field has been discussed by Bronnikov et al. [30]. Sharif and his collaborator [31] displayed the stable system of thin-shell WH corresponding to the regular charged BH for a nonlinear electrodynamics field. Similarly, many authors discussed the stability of the thin-shell WH structures against different scenarios such as electric field, several EoSs, and some other physical variables [32–51].

The stable configuration of thin-shell WH geometry is hugely influenced by the selection of BH along with the EoSs. For this purpose, enormous researchers implemented distinct EoSs to inspect the various structural aspects of WHs. Eiroa and Simeone [52] formulated the thin-shell WHs by employing the Chaplygin gas (CG) and examined their stable solutions. The stable geometry of the spherical thin-shell WH under the effect of generalized CG with the inclusion of electric charge and cosmological constant has also been observed [53]. Sharif and Azam [54, 55] adopted the charged regular BH for the production of a thin-shell WH associated with the CG as well as generalized CG. They explored the static stable solutions and exhibited the unstable/stable configurations of thin-shell WHs with cylindrical metric. Varela [56] discussed the stable solutions of thin-shell WH associated with the Schwarzschild BH by taking into account the variable EoS and displayed the perturbative interpretation of equation of motion (EoM) of WH corresponding to the variable Chaplygin EoS. Similarly, the dynamical interpretation of thin-shell WH with electric field and variable EoS has also been observed by Eid [57].

Sharif and Javed analyzed the stable thin-shell WH geometry obtained by the Bardeen BH [58] and Bardeen AdS BH [59] for several proposals of EoSs. They also showed the comparison of different WH structures for CG, phantom-like, and generalized barotropic EoSs [60]. Li et al. [61] determined the solutions for (3+1)-dimensional BH corresponding to the CG and dark fluid. They examined some structural attributes of BH solutions like pressure, shadow, thermodynamics, and critical points of temperature. Recently, Javed and his collaborators [62] inspected the stable thin-shell WH geometry for charged quantum corrected BH using barotropic, phantom, and Chaplygin variable EoS. They observed that the appearance of charge factor increases the stable configuration of WHs.

In this manuscript, we are going to inspect the stability of thin-shell WH corresponding to the charged regular BH bounded by perfect fluid dark matter (PFDM). The manuscript is displayed in the following way: The next section deals with the basic interpretation of charged regular BH, and the thin-shell WH is formulated by two equivalent copies of adopted BH with the help of cut-and-paste formalism. Section III presents the stability analysis of constructed structures through radial perturbation associated with the generalized phantom-like, barotropic, as well as the Chaplygin-like EoS. The graphical description as well as the comparison is also presented in the same section. The final section compiles our main results.

2 Construction of thin-shell wormholes

Here, we evaluate the EoM of the thin-shell WHs that are formulated by employing the two similar forms of charged Bardeen BHs. The proposed BH metric is provided by [63]

$$ds^2 = -\mathcal{W}(r)dt^2 + \frac{1}{\mathcal{W}(r)}dr^2 + r^2 d\Omega^2, \tag{1}$$

where $\mathcal{W}(r)$ denotes the lapse function which depends upon the radial parameter r and $d\theta^2 + \sin^2\theta d\phi^2 = d\Omega^2$. The mathematical form of the lapse function is presented by [63]

$$\mathcal{W}(r) = \frac{\eta \log\left(\frac{r}{|\eta|}\right)}{r} - \frac{2r^2\mathcal{M}}{\left(Q^2 + r^2\right)^{3/2}} + 1, \tag{2}$$

where $\mathcal{M}$ indicates the BH mass, and η characterizes the PFDM parameter, while Q manifests the nonlinear electromagnetic charge. Zhang et al. [63] examined the interaction between Bardeen BHs, described by the Bardeen metric, and dark matter in the form of a perfect fluid. The study investigates how the presence of dark matter in this fluid state influences the properties and behavior of Bardeen BHs. The article explored gravitational effects, energy distribution, and other relevant aspects of BHs in the context of their interaction with dark matter in a perfect fluid state [63]. Also, the absence of Q with $\eta \to 0$ leads to the Schwarzschild BH. For the limiting case $\eta \to 0$, this solution represents the Bardeen regular BH [1].

For the creation of thin-shell WHs, we adopt two equivalent forms of the considered BH metrics. After that, the cut-and-paste methodology is utilized to express the thin-shell WHs. It is widely recognized that the structure of WHs uses a tunnel known as the WH throat to connect two separate eras of spacetime. The notion of the observers traveling from one area to a different one by the WH throat is an intriguing conjecture in both fields like cosmology and astrophysics. The frequently expanding and collapsing nature of the WH throat prevents any observer from passing through it uninterrupted. In order to avoid the collapsing of WH throat, a specific type of matter configuration is required for the presence of traversable WH. Since the usual matter is not suitable for the traversable WH, therefore, some matter distribution having exotic properties must exist. The exotic matter does not obey the null as well as weak energy constraints. To minimize the quantity of such exotic content, the cut-and-paste technique is presented to generate the thin-shell WHs by compiling two BH spacetimes at the hypersurface. Here, we implement this method to construct such WH geometry possessing the nonlinear influence of electrodynamics. For this purpose, we cut the line element as $\mathcal{M}^{\pm} = \left\{r^{\pm} \leq \chi,\ \chi > r_h\right\}$, in which χ symbolizes the throat radius, whereas the event horizon radius is exhibited by r_h. Such metric is combined at (2+1)-dimensional hypersurface presented by $\Sigma = \left\{r^{\pm} = \chi,\ \chi > r_h\right\}$. Such method yields a unique regular manifold given by $\mathcal{M} = \mathcal{M}^{+} \cup \mathcal{M}^{-}$.

It is important to note that the emergence of the singularity and event horizon in the created geometry can be avoided by taking into account $\chi > r_h$. Using Darmois and Israel formalism, the constituents of manifolds and hypersurface lead to $x^{\gamma} = (t, r, \theta, \phi)$, and $\xi^{i} = (\tau, \theta, \phi)$, respectively, having τ acts as the proper time on the hypersurface. These metrics are joined with the transformation of coordinates expressed by

$$g_{ij} = \frac{\partial x^{\gamma}}{\partial \xi^{i}} \frac{\partial x^{\beta}}{\partial \xi^{j}} g_{\gamma\beta}. \tag{3}$$

The respective parametric expression for the hypersurface is illustrated by $\Sigma : R(r, \tau) = r - \chi(\tau) = 0$. In order to inspect the structure of a thin shell, we consider that the shell radius (χ) is based upon the proper time. Thus, the shell radius as a function of proper time is presented by $\chi = \chi(\tau)$. The corresponding induced metric yields

$$ds_{\Sigma}^2 = \chi^2(\tau)\sin^2\theta d\phi^2 + \chi^2(\tau)d\theta^2 - d\tau^2. \tag{4}$$

The matter constituents associated with the thin shell manifest a crucial role in stability and dynamics of the WH throat. Such matter composition creates discontinuity in the internal and external contents of extrinsic curvature that is mathematically characterized by $[K^{i}{}_{j}] = K^{+i}{}_{j} - K^{-i}{}_{j} \neq 0$. The forms of extrinsic curvature corresponding to the exterior and interior domains are as follows

$$K_{ij}^{(\pm)} = -n_{\mu}^{(\pm)}\left(\frac{\partial^2 x^{\mu}}{\partial \xi^{i}\partial \xi^{j}} + \Gamma_{\gamma\beta}^{\mu}\frac{\partial x^{\gamma}}{\partial \xi^{i}}\frac{\partial x^{\beta}}{\partial \xi^{j}}\right)_{\Sigma}. \tag{5}$$

The time dependent and radial contents of the unit normals on $\mathcal{M}^{\pm}$ provide

$$n_t^{\pm} = -\dot{\chi}, \quad n_r^{\pm} = \frac{\sqrt{\frac{\eta\log\left(\frac{\chi}{|\eta|}\right)}{\chi} + \dot{\chi}^2 - \frac{2\chi^2\mathcal{M}}{(\chi^2+Q^2)^{3/2}} + 1}}{\frac{\eta\log\left(\frac{\chi}{|\eta|}\right)}{\chi} - \frac{2\chi^2\mathcal{M}}{(\chi^2+Q^2)^{3/2}} + 1},$$

respectively, in which overdot exhibits the derivative associated with the proper time. The components of corresponding extrinsic curvature are

$$K^{\pm}_{\tau\tau} = \pm\frac{\frac{2\eta\log\left(\frac{\chi}{|\eta|}\right)}{\chi^3} - \frac{3\eta}{\chi^3} - \frac{2\mathcal{M}(2\chi^4+2Q^4-11\chi^2Q^2)}{(\chi^2+Q^2)^{7/2}}}{2\sqrt{\frac{\eta\log\left(\frac{\chi}{|\eta|}\right)}{\chi} + \dot{\chi}^2 - \frac{2\chi^2\mathcal{M}}{(\chi^2+Q^2)^{3/2}} + 1}}, \quad K^{\pm}_{\theta\theta} = \pm\chi\sqrt{\frac{\eta\log\left(\frac{\chi}{|\eta|}\right)}{\chi} + \dot{\chi}^2 - \frac{2\chi^2\mathcal{M}}{\left(\chi^2+Q^2\right)^{3/2}} + 1}, \tag{6}$$

and $K^{\pm}_{\phi\phi} = \sin^2\theta K^{\pm}_{\theta\theta}$.

In order to explain the field equations at the boundary like the BH event horizon or the boundary of a massive entity, the Lanczos equations are formulated. The matter components at the hypersurface are evaluated by the reduced forms of Einstein's equations. These equations are characterized as the Lanczos equations, given by

$$S^i{}_j = -\frac{1}{8\pi}\Big(\Big[K^i{}_j\Big] - \delta^i{}_j\, K\Big). \tag{7}$$

in which $diag(\varrho,\ \mathcal{Z},\ \mathcal{Z}) = S^i{}_j$ denotes the stress–energy tensor, $K^i{}_j$ exhibits the contents of extrinsic curvature, and K symbolizes the trace part of extrinsic curvature ($[K^i{}_i] = K$). At hypersurface, the matter energy as well as the surface pressure is manifested by ϱ and $\mathcal{Z}$, respectively. The Lanczos equation (7) along with Eq. (6) leads to

$$2\pi\chi\varrho = -\sqrt{\frac{\eta\log\left(\frac{\chi}{|\eta|}\right)}{\chi} + \dot{\chi}^2 - \frac{2\chi^2\mathcal{M}}{\left(\chi^2+Q^2\right)^{3/2}} + 1}, \quad 8\pi\chi\mathcal{Z} = \frac{\frac{\eta\log\left(\frac{\chi}{|\eta|}\right)}{\chi} + 2\dot{\chi}^2 + 2\chi\left(\ddot{\chi} - \frac{\chi\mathcal{M}(\chi^2+4Q^2)}{(\chi^2+Q^2)^{5/2}}\right) + \frac{\eta}{\chi} + 2}{\sqrt{\frac{\eta\log\left(\frac{\chi}{|\eta|}\right)}{\chi} + \dot{\chi}^2 - \frac{2\chi^2\mathcal{M}}{(\chi^2+Q^2)^{3/2}} + 1}}. \tag{8}$$

At this place, we assume that at the shell's equilibrium radius, χ_0, the shell of the developed structure does not move across the radial direction. Therefore, it is important to note that the proper time derivative of the shell's radius vanishes, i.e., $\dot{\chi_0} = 0 = \ddot{\chi_0}$. We have

$$2\pi\chi_0\varrho_0 = -\sqrt{\frac{\eta\log\left(\frac{\chi_0}{|\eta|}\right)}{\chi_0} - \frac{2\chi_0^2\mathcal{M}}{\left(\chi_0^2+Q^2\right)^{3/2}} + 1}, \quad 8\pi\chi_0\mathcal{Z}_0 = \frac{\frac{\eta\log\left(\frac{\chi_0}{|\eta|}\right)}{\chi_0} + \frac{\eta}{\chi_0} - \frac{2\mathcal{M}(\chi_0^4+4\chi_0^2Q^2)}{(\chi_0^2+Q^2)^{5/2}} + 2}{\sqrt{\frac{\eta\log\left(\frac{\chi_0}{|\eta|}\right)}{\chi_0} - \frac{2\chi_0^2\mathcal{M}}{(\chi_0^2+Q^2)^{3/2}} + 1}}, \tag{9}$$

in which ϱ_0 and $\mathcal{Z}_0$ reveal the matter density and pressure at equilibrium points, respectively. Here, we have three energy bounds, i.e., weak ($\mathcal{Z}+\varrho \geq 0,\ \varrho \geq 0$), null ($\mathcal{Z}+\varrho \geq 0$), and strong ($3\mathcal{Z}+\varrho \geq 0$). Note that $\varrho_0 < 0$ yields the defiance of weak as well as dominant energy bounds. Such nullification depicts the occurrence of exotic content in the created geometry. Such substance in the throat produces aversion of collapse and assists in keeping it open. Hence, our developed geometry portrays physically acceptable structure for the WH.

The EoS by considering the shell density (8) provides $\dot{\chi}^2 = -\Psi(\chi)$, while the effective potential of the shell is of the form

$$\Psi(\chi) = \frac{\eta\log\left(\frac{\chi}{|\eta|}\right)}{\chi} - 4\pi^2\chi^2\varrho(\chi)^2 - \frac{2\chi^2\mathcal{M}}{\left(\chi^2+Q^2\right)^{3/2}} + 1. \tag{10}$$

The repulsive and attractive attributes of WH throat in accordance with the 4-acceleration are presented by

$$a^\beta = v^\beta_{;\chi}\, v^\chi,$$

in which the 4-velocity becomes $v^\chi = \left(\frac{1}{\sqrt{\mathcal{W}(r)}},\ 0,\ 0,\ 0\right)$. One can obtain

$$\frac{\mathrm{d}^2r}{\mathrm{d}\tau^2} = -\Gamma^r_{tt}\left(\frac{\mathrm{d}t}{\mathrm{d}\tau}\right)^2 = -a^r,$$

providing

$$a^r = \frac{\eta\log(|\eta|) - \eta\log(\chi) + \eta + \frac{2\chi^3\mathcal{M}(\chi^2-2Q^2)}{(\chi^2+Q^2)^{5/2}}}{2\chi^2}.$$

It is well known that the gravitational field creates two kinds of behavior repulsive or attractive around the WHs. In repulsive behavior, the gravitational field of WH repels the objects. In this situation, an observer needs to exert an inwardly directed force to prevent being pushed by the WH. They can combat the repellent gravitational pull and maintain their distance from the WH by applying this force in its direction. They will be driven further away from the WH if they do not provide this inward force. On the

other hand, the gravitational field of an attractive WH attracts the objects towards it. In this situation, an observer must produce an outward-directed force in order to prevent being drawn into the WH. They must therefore depart from the WH with a force that repels the gravitational attraction. They will eventually be pulled towards the WH if they do not use this outward force. In short, the repulsive or attractive features of gravitational field of WHs suggest the sort of force that an observer requires to employ to prevent being affected by the WH. Thus, a repulsive WH needs an inward force, while the attractive one needs an outward force. The radial factor of the 4-acceleration narrates the repulsive ($a^r < 0$) and attractive ($a^r > 0$) natures of the throat.

3 Stability analysis

To inspect the stability of WH geometry, we adopt the shell's equilibrium radius χ_0 and expand the effective potential $\Psi(\chi)$ about χ_0 using Taylor series up to second order as

$$\Psi(\chi) = \Psi(\chi_0) + \Psi'(\chi_0)(\chi - \chi_0) + \frac{1}{2}\Psi''(\chi_0)(\chi - \chi_0)^2 + O[(\chi - \chi_0)^3]. \tag{11}$$

Here, dash represents the derivative with respect to shell radius χ. It is interesting to mention that for both geometries (unstable or stable) of WH, the throat requires the disappearance of potential constituent and its first derivative at the equilibrium state, i.e., $\Psi(\chi_0) = 0 = \Psi'(\chi_0)$. Hence, it can be evaluated as:

- For $\Psi''(\chi_0) > 0$, we obtain the stable geometry and $\Psi''(\chi_0) < 0$ corresponds the unstable geometry.
- It is neither unstable nor stable for $\Psi''(\chi_0) = 0$.

At the state of equilibrium, Eq. (11) yields

$$\Psi(\chi) = \frac{1}{2}\Psi''(\chi_0)(\chi - \chi_0)^2. \tag{12}$$

As the conservation law is obeyed by $\mathcal{Z}$ and ϱ which is given as

$$\mathcal{Z}\frac{\mathrm{d}}{\mathrm{d}\tau}(4\pi\chi^2) + \frac{\mathrm{d}}{\mathrm{d}\tau}(4\pi\chi^2\varrho) = 0. \tag{13}$$

The accurate solution of the conservation equation depends on the choice of matter composition that can be described by EoS. Here, we implement two EoSs $\mathcal{Z} = \mathcal{Z}(\varrho)$ and $\mathcal{Z} = \mathcal{Z}(\varrho, \chi)$. The later displays the generalized expression in which the surface pressure of the shell relies on the surface density as well as the throat radius. Corresponding to both, we obtain $\mathcal{Z}' = \frac{d\mathcal{Z}(\varrho)}{d\varrho}\varrho'$ and $\mathcal{Z}' = \frac{d\mathcal{Z}}{d\varrho}\varrho' + \frac{d\mathcal{Z}}{d\chi}$, respectively. So, the conservation equation provides

$$\varrho' = -\frac{2}{\chi}\{\varrho + \mathcal{Z}(\varrho, \chi)\}. \tag{14}$$

Equation (14) generates a specific form of $\Psi(\chi)$ with respect to distinct choices of variable EoS. At $\chi = \chi_0$, the 2^{nd} derivative of effective potential takes the form

$$\begin{aligned}\Psi''(\chi_0) =& \frac{2\eta\log\left(\frac{\chi_0\mathrm{sgn}(\eta)}{\eta}\right)}{\chi_0^3} - \frac{3\eta}{\chi_0^3} - 8\pi^2\left(\chi_0^2\varrho'(\chi_0)^2 + \chi_0\varrho(\chi_0)\left(\chi_0\varrho''(\chi_0) + 4\varrho'(\chi_0)\right) + \varrho(\chi_0)^2\right) \\ &- \frac{2\mathcal{M}\left(\chi_0^2 + Q^2\right)^{-7/2}}{\left(2\chi_0^4 + 2Q^4 - 11\chi_0^2Q^2\right)^{-1}}.\end{aligned} \tag{15}$$

This expression and Eq. (14) interpret the matter components placed at thin shell and contribute a marvelous role to inspect the stable configurations of the developed geometry. Next sections are devoted to discuss the impacts of barotropic as well as variable EoS on the stability of the created geometry.

3.1 Barotropic EoS

In order to analyze the stable structure of thin-shell WH, we first consider the barotropic EoS. This EoS connects the surface pressure and energy density of matter by $\mathcal{Z} = \Theta\varrho$, in which Θ indicates the parameter for barotropic EoS. Employing this EoS in (14), we obtain

$$\varrho'(\chi) = -\frac{2}{\chi}(1 + \Theta)\varrho(\chi), \tag{16}$$

providing

$$\varrho(\chi) = \varrho(\chi_0)\left(\frac{\chi_0}{\chi}\right)^{2(1+\Theta)}. \tag{17}$$

The expression for effective potential leads to

$$\Psi(\chi)=\frac{\eta\log\left(\frac{\chi}{|\eta|}\right)}{\chi}-4\pi^2\chi^2\left(\varrho_0\left(\frac{\chi_0}{\chi}\right)^{2(\Theta+1)}\right)^2-\frac{2\chi^2\mathcal{M}}{\left(\chi^2+Q^2\right)^{3/2}}+1, \tag{18}$$

At χ_0, the expression of first differential corresponding to throat radius "χ"yields

$$\Psi'(\chi_0)=\frac{(4\Theta\eta+\eta)\log\left(\frac{\chi_0}{|\eta|}\right)+(4\Theta+2)\chi_0+\eta-\frac{2\chi_0^5(4\Theta\mathcal{M}+\mathcal{M})}{\left(\chi_0^2+Q^2\right)^{5/2}}-\frac{8(\Theta+1)\chi_0^3Q^2\mathcal{M}}{\left(\chi_0^2+Q^2\right)^{5/2}}}{\chi_0^2}.$$

It is noted that $\Psi'(\chi_0)$ vanishes if and only if

$$\Theta=-\frac{\eta\log\left(\frac{\chi_0}{|\eta|}\right)+2\chi_0+\eta-\frac{2\chi_0^5\mathcal{M}}{\left(\chi_0^2+Q^2\right)^{5/2}}-\frac{8\chi_0^3Q^2\mathcal{M}}{\left(\chi_0^2+Q^2\right)^{5/2}}}{4\left(\eta\log\left(\frac{\chi_0}{|\eta|}\right)+\chi_0-\frac{2\chi_0^3\mathcal{M}}{\left(\chi_0^2+Q^2\right)^{3/2}}\right)}. \tag{19}$$

Also, it is found that

$$\begin{aligned}\Psi''(\chi_0)=&-\frac{3\eta}{\chi_0^3}+\frac{2\mathcal{M}\left(4(\Theta+1)(4\Theta+1)\chi_0^4+4(\Theta+1)(4\Theta+1)Q^4+(8\Theta(4\Theta+5)+23)\chi_0^2Q^2\right)}{\left(\chi_0^2+Q^2\right)^{7/2}}\\&-\frac{4(\Theta+1)(4\Theta+1)\eta\log\left(\frac{\chi_0}{|\eta|}\right)}{\chi_0^3}-\frac{2(2\Theta+1)(4\Theta+3)}{\chi_0^2}.\end{aligned} \tag{20}$$

This equation exhibits a significant role in discussing the dynamical composition of thin-shell WH in the light of barotropic EoS.

3.2 Phantom-like variable EoS

Secondly, we choose the phantom-like variable EoS to examine the stability of thin-shell WH structures. This EoS is expressed as $\mathcal{Z}=\frac{\mathcal{D}}{\chi^n}\varrho$, along with $\mathcal{D}$ as the EoS parameter, and n depicts the real constant. This expression displays the extended form of phantom-like EoS. For $n\to 0$, it corresponds to phantom-like. Utilizing this EoS, the conservation equation takes the form

$$\varrho(\chi)=\varrho_0 e^{\frac{2\mathcal{D}}{n}\left(\frac{1}{\chi^n}-\frac{1}{\chi_0^n}\right)}\left(\frac{\chi_0}{\chi}\right)^2. \tag{21}$$

The effective potential provides

$$\Psi(\chi)=-4\pi^2\chi^2\varrho_0^2\left(\frac{\chi_0}{\chi}\right)^4 e^{\frac{(2\mathcal{D})\left(\frac{1}{\chi^n}-\frac{1}{\chi_0^n}\right)}{n}}+\frac{\eta\log\left(\frac{\chi}{|\eta|}\right)}{\chi}-\frac{2\chi^2\mathcal{M}}{\left(\chi^2+Q^2\right)^{3/2}}+1. \tag{22}$$

Observe that the effective potential vanishes at $\chi=\chi_0$ and the first differential form is derived as

$$\Psi'(\chi_0)=\frac{\left(2\mathcal{D}\eta\chi_0^{-n}+\eta\right)\log\left(\frac{\chi_0}{|\eta|}\right)+2\chi_0\left(\mathcal{D}\chi_0^{-n}\left(1-\frac{2\chi_0^2\mathcal{M}}{\left(\chi_0^2+Q^2\right)^{3/2}}\right)-\frac{\mathcal{M}(\chi_0^4+4\chi_0^2Q^2)}{\left(\chi_0^2+Q^2\right)^{5/2}}+1\right)+\eta}{\chi_0^2}, \tag{23}$$

By taking $\Psi'(\chi_0)=0$, we obtain

$$\mathcal{D}=-\frac{\chi_0^n\left(\eta\log\left(\frac{\chi_0}{|\eta|}\right)+2\chi_0+\eta-\frac{2\chi_0^3\mathcal{M}(\chi_0^2+4Q^2)}{\left(\chi_0^2+Q^2\right)^{5/2}}\right)}{2\left(\eta\log\left(\frac{\chi_0}{|\eta|}\right)+\chi_0-\frac{2\chi_0^3\mathcal{M}}{\left(\chi_0^2+Q^2\right)^{3/2}}\right)}. \tag{24}$$

Hence, we have

$$\begin{aligned}\Psi''(\chi_0)=&-2\chi_0^{-2(n+1)}\left(2\mathcal{D}^2+\mathcal{D}(n+5)\chi_0^n+3\chi_0^{2n}\right)\left(\frac{\eta\log\left(\frac{\chi_0}{|\eta|}\right)}{\chi_0}-\frac{2\chi_0^2\mathcal{M}}{\left(\chi_0^2+Q^2\right)^{3/2}}+1\right)+\frac{2\eta\log\left(\frac{\chi_0}{|\eta|}\right)}{\chi_0^3}-\frac{3\eta}{\chi_0^3}\\&-\frac{2\mathcal{M}\left(2\chi_0^4+2Q^4-11\chi_0^2Q^2\right)}{\left(\chi_0^2+Q^2\right)^{7/2}}.\end{aligned} \tag{25}$$

3.3 Chaplygin variable EoS

Here, the Chaplygin variable EoS is adopted which is illustrated by $\mathcal{Z} = \frac{1}{\chi^n}\frac{\mathcal{H}}{\varrho}$, where $\mathcal{H}$ symbolizes the EoS factor. For $n \to 0$, this reduces to Chaplygin EoS. In accordance with surface density, the conservation equation yields

$$\varrho^2(\chi) = \frac{4\mathcal{H}\left(\chi^4\chi_0^n - \chi^n\chi_0^4\right) + \varrho_0^2\chi_0^{n+4}\chi^n(n-4)}{(n-4)\chi^{n+4}\chi_0^n}. \tag{26}$$

The potential function provides $\Psi(\chi_0) = 0$. Moreover, $\Psi'(\chi)$ is evaluated and implementing $\Psi'(\chi_0) = 0$, we have

$$\mathcal{H} = \frac{\chi_0^{n-1}\left(-\frac{\eta\log\left(\frac{\chi_0}{|\eta|}\right)+2\chi_0+\eta}{\chi_0^2} + \frac{8\chi_0\mathcal{M}}{(\chi_0^2+Q^2)^{3/2}} - \frac{6\chi_0^3\mathcal{M}}{(\chi_0^2+Q^2)^{5/2}}\right)}{16\pi^2}. \tag{27}$$

At $\chi = \chi_0$, the second derivative of effective potential corresponding to shell radius is given by

$$\Psi''(\chi_0) = -\frac{(n+1)\left(-\frac{\eta\log\left(\frac{\chi_0}{|\eta|}\right)+2\chi_0+\eta}{\chi_0^2} + \frac{8\chi_0\mathcal{M}}{(\chi_0^2+Q^2)^{3/2}} - \frac{6\chi_0^3\mathcal{M}}{(\chi_0^2+Q^2)^{5/2}}\right)}{\chi_0} + \frac{46\chi_0^2Q^2\mathcal{M}}{(\chi_0^2+Q^2)^{7/2}} + \frac{8\chi_0^4\mathcal{M}}{(\chi_0^2+Q^2)^{7/2}} + \frac{8Q^4\mathcal{M}}{(\chi_0^2+Q^2)^{7/2}}$$
$$- \frac{6\chi_0 + 3\eta + 4\eta\log\left(\frac{\chi_0\mathrm{sgn}(\eta)}{\eta}\right)}{\chi_0^3}. \tag{28}$$

In the following subsection, the detail discussion is presented which illustrates the impact of PFDM as well as variable EoS on the stable configurations of thin-shell WHs.

3.4 Graphical analysis and comparison

Now, we present the detail effects of PFDM and different choices of EoS on the stability of the developed thin-shell WHs. In this respect, we consider Schwarzschild BH, Schwarzschild BH with PFDM, Bardeen BH and Bardeen BH with PFDM for respective values of physical parameters as $\eta = 0 = Q$, $\eta \neq 0$, $Q = 0$, $\eta = 0$, $Q \neq 0$, and $\eta \neq 0$, $Q \neq 0$, respectively. For these choices, the respective position of the event horizon is also calculated with specific values of physical parameters. Then, we perturb our system about equilibrium shell radius. By implementing the fundamental constraint of thin-shell WH that the shell radius should be larger than the position of the event horizon, we use $\chi_0 = r_h + \varepsilon$ for every case where $0 < \varepsilon \ll 1$ is a very small positive real constant. Then, we consider the final expressions of second derivative of potential functions of barotropic, Chaplygin, and phantom-like variable EoS to obtain the stability in the framework of with and without PFDM parameter. The final outcomes of the developed thin-shell WHs for distinct values of BH spacetimes are given as follows:

3.4.1 For Schwarzschild BH

We begin the analysis for Schwarzschild BH for considered choices of EoS. The detail description of stable/unstable configuration associated with feasible choices of physical parameter by employing the location of event horizon is given in Table 1. We consider the thin-shell WH constraints $\chi_0 > r_h$. In this regard, we use $\chi_0 = 2 + \varepsilon$ with event horizon 2 of Schwarzschild BH for the physical parameters $\mathcal{M} = 1$, $Q = 0$, $\eta = 0$. Table 1 depicts the unstable configuration for barotropic EoS and phantom-like variable EoS for all choices of n. The developed structure for the Schwarzschild BH shows stable configuration for Chaplygin variable EoS if $n \geq 0.7228$ which is also shown in the left plot of Fig. 1. The respective values of $\Psi''(\mathcal{E}) > 1$ for Chaplygin variable EoS with specific values of $\mathcal{E}$ for $n = 1$ are shown in Table 1. Right plot of Fig. 1 represents the completely unstable configurations for phantom-like variable EoS for every values of n presented in Table 1. Hence, for the choice of Schwarzschild BH, thin-shell WHs only show stable structure for Chaplygin variable EoS for $n \geq 0.7228$ and unstable for every choice of barotropic as well as phantom-like variable EoS $\forall n$.

3.4.2 For Schwarzschild BH with PFDM

Secondly, we consider the choice of Schwarzschild BH surrounded by PFDM as shown in Table 2 and Fig. 2. It is found that PFDM greatly affects the stability of the constructed geometry. In the presence of PFDM, thin-shell WHs show stable configurations for Chaplygin (with $n > 1.38$) as well as phantom-like (with $n > 0.3352$) variable EoS and found unstable configuration for barotropic EOS. In the presence of PFDM, the stability configuration is obtained for higher values of n in the framework of Chaplygin variable fluid as compared to the Schwarzschild BH. But, PFDM also provides the possibility of stability for smallest values of n for phantom-like variable EoS (Table 2 and Fig. 2).

Table 1 Effects of different EoSs on the stability of thin-shell WHs for Schwarzschild BHs with $\eta = 0$, $\mathcal{M} = 1$, $Q = 0$, $\chi_0 = \varepsilon + 2$. Here, we use variable EoS (VEoS). We observe the behavior of potential function second derivative by using the constraint $\chi_0 = r_h + \varepsilon$, where $r_h = 2$ is the radius of event horizon of Schwarzschild BH

$\mathcal{E}$	Barotropic EoS $\Psi''(\mathcal{E}) < 0$	Chaplygin VEoS For $(n = 0.5)$ $\Psi''(\mathcal{E}) < 0$	Chaplygin VEoS For $(n = 1)$ $\Psi''(\mathcal{E}) > 0$	phantom-like VEoS For $(n = 2)$ $\Psi''(\mathcal{E}) < 0$	phantom-like VEoS For $(n = 2.2)$ $\Psi''(\mathcal{E}) < 0$
0.0001	− 1.70423	− 0.0502211	0.065499	− 1.68109	− 1.19506
0.0006	− 1.69958	− 0.050395	0.0653043	− 1.67645	− 1.19051
0.0011	− 1.69496	− 0.0505687	0.0651098	− 1.67182	− 1.18597
0.0016	− 1.69036	− 0.0507422	0.0649156	− 1.66723	− 1.18146
0.0021	− 1.68578	− 0.0509153	0.0647217	− 1.66265	− 1.17697
0.0026	− 1.68122	− 0.0510881	0.0645281	− 1.65809	− 1.1725
0.0031	− 1.67668	− 0.0512607	0.0643347	− 1.65356	− 1.16806
0.0036	− 1.67216	− 0.0514329	0.0641416	− 1.64905	− 1.16363
0.0041	− 1.66766	− 0.0516049	0.0639488	− 1.64455	− 1.15923
0.0046	− 1.66319	− 0.0517766	0.0637562	− 1.64008	− 1.15484

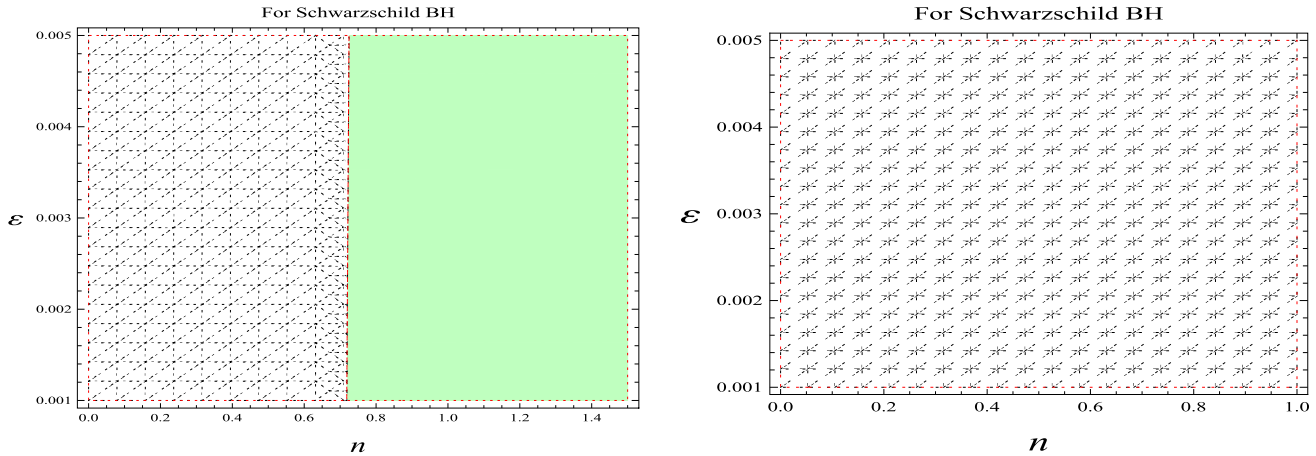

Fig. 1 Stability configurations of Schwarzschild BH ($\eta = 0 = Q$) for Chaplygin variable EoS (left plot) and phantom-like variable EoS (right plot) with $\mathcal{M} = 1$, $Q = 0$, $\chi_0 = \varepsilon + 2$. The shaded green regions show the stable regions ($\Psi''(\chi_0) > 0$), and white doted regions show unstable configurations ($\Psi''(\chi_0) \leq 0$) configurations

Table 2 Effects of different EoSs on the stability of thin-shell WHs for Schwarzschild BHs with PFDM for $\mathcal{M} = 1$, $Q = 0$, $\eta = 1$, $\chi_0 = \varepsilon + 4.41421$. We observe the behavior of potential function second derivative by using the constraint $\chi_0 = r_h + \varepsilon$, where $r_h = 4.41421$ is the radius of event horizon of Schwarzschild BH with PFDM

$\mathcal{E}$	Barotropic EoS $\Psi''(\mathcal{E}) < 0$	Chaplygin VEoS For $(n = 1)$ $\Psi''(\mathcal{E}) < 0$	Chaplygin VEoS For $(n = 2)$ $\Psi''(\mathcal{E}) > 0$	Phantom-like VEoS For $(n = 0.1)$ $\Psi''(\mathcal{E}) < 0$	Phantom-like VEoS For $(n = 0.5)$ $\Psi''(\mathcal{E}) > 0$
0.0001	− 0.0360844	− 0.102285	0.00598883	− 0.025257	0.0180524
0.0006	− 0.0360687	− 0.102264	0.00598548	− 0.0252437	0.0180562
0.0011	− 0.036053	− 0.102244	0.00598213	− 0.0252305	0.0180599
0.0016	− 0.0360374	− 0.102223	0.00597879	− 0.0252172	0.0180636
0.0021	− 0.0360217	− 0.102203	0.00597544	− 0.0252039	0.0180674
0.0026	− 0.0360061	− 0.102182	0.0059721	− 0.0251907	0.0180711
0.0031	− 0.0359905	− 0.102162	0.00596876	− 0.0251774	0.0180748
0.0036	− 0.0359748	− 0.102141	0.00596542	− 0.0251642	0.0180786
0.0041	− 0.0359592	− 0.102121	0.00596208	− 0.0251509	0.0180823
0.0046	− 0.0359436	− 0.1021	0.00595875	− 0.0251377	0.018086

3.4.3 For Bardeen BH

Thirdly, we are interested to observe the stable structure of thin-shell WHs in the context of Bardeen BHs. It is obtained that the constructed structure shows completely unstable configuration for barotropic EoS and phantom-like variable EoS $\forall n$ as shown in Table 3 and Fig. 3. Bardeen thin-shell WHs show stability only for Chaplygin variable EoS if $n \geq 0.2708$. Hence, it is noteworthy that the presence of regular BH increases the stability criteria for smaller values of n as compared to the Schwarzschild BH with and without PFDM.

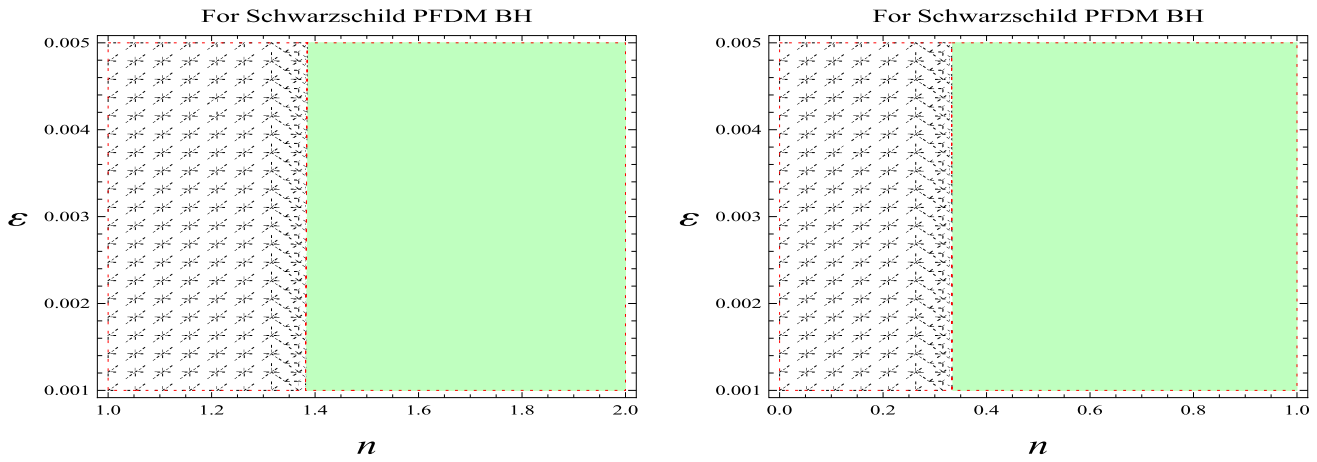

Fig. 2 Stability configurations of Schwarzschild BH with PFDM ($\eta \neq 0,\ Q = 0$) for Chaplygin variable EoS (left plot) and phantom-like variable EoS (right plot) with $\mathcal{M} = 1,\ Q = 0,\ \eta = 1,\ \chi_0 = \varepsilon + 4.41421$

Table 3 Effects of different EoSs on the stability of thin-shell WHs for Bardeen BHs with $\eta = 0$, $\mathcal{M} = 1,\ Q = 0.5$, $\chi_0 = \varepsilon + 1.78597$. Here, we use variable EoS (VEoS). We observe the behavior of potential function second derivative by using the constraint $\chi_0 = r_h + \varepsilon$, where $r_h = 1.78597$ is the radius of event horizon of Bardeen BH

$\mathcal{E}$	Barotropic EoS $\Psi''(\mathcal{E}) < 0$	Chaplygin VEoS For $(n = 0.1)$ $\Psi''(\mathcal{E}) < 0$	Chaplygin VEoS For $(n = 0.5)$ $\Psi''(\mathcal{E}) > 0$	Phantom-like VEoS For $(n = 0.5)$ $\Psi''(\mathcal{E}) < 0$	Phantom-like VEoS For $(n = 2.2)$ $\Psi''(\mathcal{E}) < 0$
0.0001	− 4343.64	− 0.0404701	0.0575892	− 4377.91	− 4377.4
0.0006	− 729.289	− 0.0408117	0.0572404	− 729.298	− 728.783
0.0011	− 397.632	− 0.0411526	0.0568921	− 397.606	− 397.091
0.0016	− 273.246	− 0.041493	0.0565444	− 273.222	− 272.707
0.0021	− 208.093	− 0.0418327	0.0561972	− 208.068	− 207.553
0.0026	− 167.998	− 0.0421719	0.0558506	− 167.974	− 167.459
0.0031	− 140.837	− 0.0425105	0.0555046	− 140.813	− 140.298
0.0036	− 121.221	− 0.0428484	0.0551591	− 121.197	− 120.682
0.0041	− 106.39	− 0.0431858	0.0548142	− 106.365	− 105.851
0.0046	− 94.7826	− 0.0435226	0.0544698	− 94.758	− 94.2436

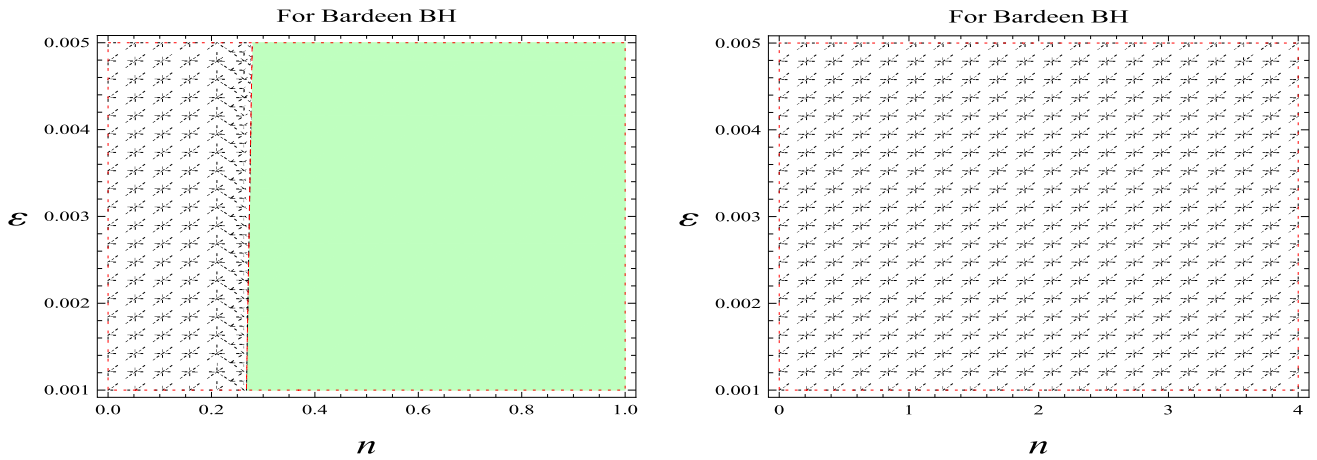

Fig. 3 Stability configurations of Bardeen BH ($\eta = 0,\ Q \neq 0$) for Chaplygin variable EoS (left plot) and phantom-like variable EoS (right plot) with $\mathcal{M} = 1,\ Q = 0.5,\ \chi_0 = \varepsilon + 1.78597,$. The shaded green regions show the stable regions ($\Psi''(\chi_0) > 0$),and white doted regions show unstable configurations ($\Psi''(\chi_0) \leq 0$) configurations

3.4.4 For Bardeen BH with PFDM

Finally, we consider the thin-shell WHs developed from Bardeen BH surrounded by PFDM. It is found that this type of developed structure is stable for both Chaplygin (with $n \geq 1.934$) as well as phantom-like (with $n \geq 0.2919$) variable EoS as shown in Table 4 and Fig. 4. It also represents the unstable configuration for the choice of barotropic EoS. Figure 4 explains that in the presence

Table 4 Effects of different EoSs on the stability of thin-shell WHs for Bardeen BHs with PFDM for $\mathcal{M}=1,\ Q=0.5,\ \eta=1,$ $\chi_0=\varepsilon+4.44045$. Here, we use variable EoS (VEoS). We observe the behavior of potential function second derivative by using the constraint $\chi_0=r_h+\varepsilon$, where $r_h=4.44045$ is the radius of event horizon of Bardeen BH with PFDM

$\mathcal{E}$	Barotropic EoS $\Psi''(\mathcal{E})<0$	Chaplygin VEoS For $(n=1)$ $\Psi''(\mathcal{E})<0$	Chaplygin VEoS For $(n=2.2)$ $\Psi''(\mathcal{E})>0$	Phantom-like VEoS For $(n=0.1)$ $\Psi''(\mathcal{E})<0$	Phantom-like VEoS For $(n=0.29)$ $\Psi''(\mathcal{E})>0$
0.0001	− 0.0305393	− 0.0995996	0.0283427	− 0.0198774	0.000380108
0.0006	− 0.0305269	− 0.0995803	0.0283342	− 0.0198674	0.000385734
0.0011	− 0.0305146	− 0.0995609	0.0283257	− 0.0198574	0.000391356
0.0016	− 0.0305022	− 0.0995416	0.0283171	− 0.0198473	0.000396973
0.0021	− 0.0304899	− 0.0995223	0.0283086	− 0.0198373	0.000402587
0.0026	− 0.0304776	− 0.0995031	0.0283	− 0.0198273	0.000408195
0.0031	− 0.0304652	− 0.0994838	0.0282915	− 0.0198173	0.0004138
0.0036	− 0.0304529	− 0.0994645	0.028283	− 0.0198073	0.0004194
0.0041	− 0.0304406	− 0.0994452	0.0282745	− 0.0197973	0.000424996
0.0046	− 0.0304283	− 0.0994259	0.028266	− 0.0197873	0.000430587

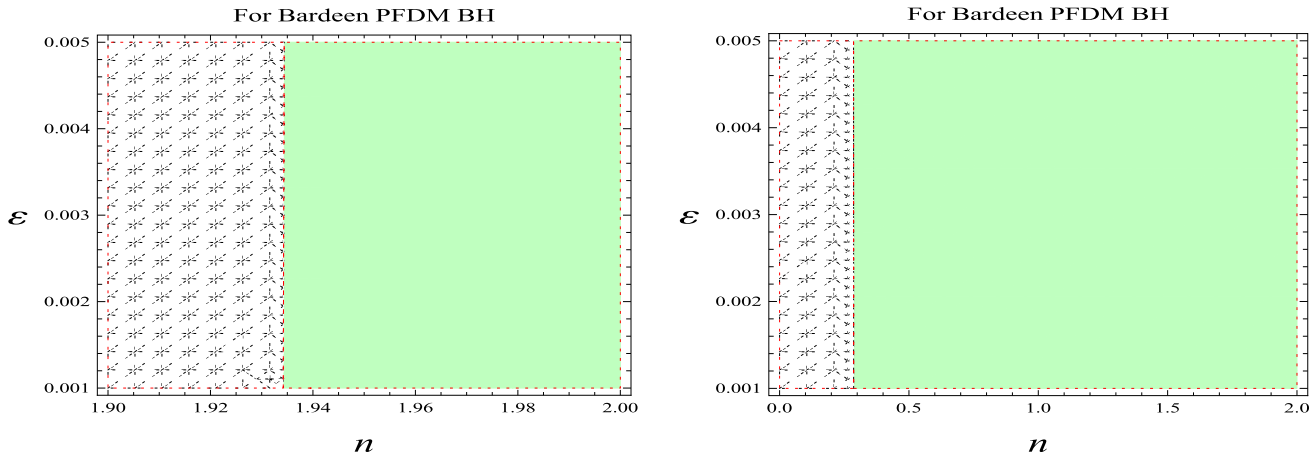

Fig. 4 Stability configurations of Bardeen BH with PFDM ($\eta\neq 0,\ Q\neq 0$) for Chaplygin variable EoS (left plot) and phantom-like variable EoS (right plot) with $\mathcal{M}=1,\ Q=0.5,\ \eta=1,\ \chi_0=\varepsilon+4.44045$

of PFDM in Bardeen thin-shell WHs, the stability criteria for Chaplygin variable EoS depend on slightly higher values of n that behave as similar as mentioned for the Schwarzschild PFDM.

4 Concluding remarks

In the framework of PFDM, this study examines the development and stability of Bardeen thin-shell WHs. The cut-and-paste methodology is used to construct thin-shell WHs using equivalent copies of Bardeen BHs with PFDM. The primary goal of the work is to use the linearized radial perturbation analysis to look into the stability of these WHs. The stability of the WHs is examined in relation to variable EoS, such as barotropic, variable Chaplygin, and phantom-like EoSs.

The discussion starts by considering the choice of Schwarzschild BHs for the EoS under consideration. The paper presents a thorough description of stable and unstable configurations for appropriate physical parameter values utilizing the event horizon location. If the parameter n is larger than or equal to 0.7228, thin-shell WHs exhibit a stable configuration for Chaplygin variable EoS (Table 1 and Fig. 1). However, for all values of n, the configurations are unstable for any combination of barotropic and phantom-like variable EoS. The research then analyzes the selection of Schwarzschild BHs encircled by PFDM. It has been shown that the created structure's stability is significantly impacted by the existence of PFDM. In the presence of PFDM, thin-shell WHs exhibit stable structures for Chaplygin (with $n\geq 1.38$) and phantom-like (with $n\geq 0.3352$) variable EoSs, while unstable topologies for barotropic EoS (Table 2 and Fig. 2). Schwarzschild BHs have a greater stability structure as compared to the Chaplygin variable fluid. For the choice of phantom-like variable EoS, Schwarzschild BH with PFDM possesses stability for lesser values of n.

Next, in the context of Bardeen BHs, the study investigates the stability of thin-shell WHs. For both barotropic and phantom-like variable EoS, the analysis demonstrates that the produced structure is entirely unstable for all values of n. Bardeen thin-shell WHs, on the other hand, only exhibit stability for the Chaplygin variable EoS if n is higher than or equal to 0.2708 (Table 3 and Fig. 3). When compared to Schwarzschild BHs with and without PFDM, the inclusion of normal BHs raises the stability requirements for

smaller values of n. The research also takes into account the thin-shell WHs created by Bardeen BHs that are encircled by PFDM. According to the research, this particular created structure is stable for both Chaplygin-like and phantom-like variable EoS (with $n \geq 1.934$ and $n \geq 0.2919$) (Table 4 and Fig. 4). In spite of this, it indicates an unstable configuration for the selected barotropic EoS. Depending on somewhat larger values of n, PFDM in Bardeen thin-shell WHs, like Schwarzschild PFDM, raises the stability criterion for Chaplygin variable EoS (Tables 1, 2, 3, 4).

The stability of thin-shell wormholes around Schwarzschild and Bardeen black holes in PFDM settings is examined in this work. It investigates the effects on the stability of these structures of various equations of state (EoS), such as barotropic, Chaplygin, and phantom-like variable EoSs. The findings indicate that in the presence of PFDM, thin-shell wormholes display unstable configurations for barotropic EoS, but stability for Chaplygin (with $n \geq 1.38$) and phantom-like (with $n \geq 0.3352$) variable EoSs. The study concludes that thin-shell wormholes are completely unstable for barotropic EoS across all black hole geometries, but they are stable for phantom-like variable EoS only in the presence of PFDM, highlighting the substantial impact of PFDM on the stability of these structures. Further investigation into the effects of various BH geometries on stability, additional variables affecting wormhole characteristics, and numerical simulations to confirm and supplement the analytical results are possible future research directions that could lead to a better understanding of gravitational physics and the stability of wormhole structures in the context of PFDM.

Acknowledgements The work was supported in part by NSFC under grants 12 271 488, 11 975 145, and 11 972 291, the Ministry of Science and Technology of China (G2021016032L and G2023016011L), and the Natural Science Foundation for Colleges and Universities in Jiangsu Province (17 KJB 110 020). Faisal Javed acknowledges Grant No. YS304023917 to support his Postdoctoral Fellowship at Zhejiang Normal University.

Data Availability Statement This manuscript has associated data in a data repository. [Authors' comment: There are no observational data related to this article. The necessary calculations and graphic discussion can be made available on request.]

Declarations

Conflict of interest The authors declare that they have no known competing financial interests or personal relationships that could have appeared to influence the work reported in this paper.

References

1. J.M. Bardeen, Proceedings of GR5 (Tiflis, USSR, 1968) 174
2. E. AyónBeato, Asymptotic Behavior of Scalar Fields Coupled to Gravity, Graduate Dissertation, Faculty of Physics (Havana Univ., 1993)
3. A. Borde, Phys. Rev. D **50**, 3392 (1994)
4. C. Barrabès, V.P. Frolov, Phys. Rev. D **53**, 3215 (1996)
5. M. Cataldo, A. García, A. Phys. Rev. D **61**, 084003 (2000)
6. I. Dymnikova, Class. Quantum Grav. **21**, 4417 (2004)
7. S. Hayward, Phys. Rev. Lett. **96**, 031103 (2006)
8. W. Berej et al., Gen. Relativ. Gravit. **38**, 885 (2006)
9. S.G. Ghosh, S.D. Maharaj, Eur. Phys. J. C **75**, 7 (2015)
10. L. Flamm, Phys. Z. **17**, 448 (1916)
11. A. Einstein, N. Rosen, Phys. Rev. **48**, 73–77 (1935)
12. R.W. Fuller, J.A. Wheeler, Phys. Rev. **128**, 919–929 (1962)
13. J.L. Blazquez-Salcedo, C. Knoll, E. Radu, Phys. Rev. Lett. **126**, 101102 (2021)
14. R.A. Konoplya, A. Zhidenko, Phys. Rev. Lett. **128**, 091104 (2022)
15. Y.Q. Wang, S.W. Wei, Y. X. Liu, Comment on Traversable Wormholes in General Relativity, [arXiv:2206.12250 [gr-qc]] (2022)
16. M.S. Morris, K.S. Thorne, Am. J. Phys. **56**, 395 (1988)
17. M. Visser, *Lorentzian Wormholes* (AIP Press, New York, 1996)
18. M.S. Morris, K.S. Thorne, U. Yurtsever, Phys. Rev. Lett. **61**, 1446 (1988)
19. J.P.S. Lemos, F.S.N. Lobo, Q. de Oliveira, S. Phys, Rev. D **68**, 064004 (2003)
20. M. Visser, Nucl. Phys. B **328**, 203 (1989)
21. M. Visser, Phys. Rev. D **39**, 3182 (1989)
22. W. Israel, Nuovo Cimento B **44**, 1 (1966)
23. A. Papapetrou, A. Hamoui, Ann. Inst. Henri Poincare **9**, 179 (1968)
24. N. Sen, Ann. Phys. (Leipzig) **73**, 365 (1924)
25. K. Lanczos, Ann. Phys. **74**, 518 (1924)
26. P. Musgrave, K. Lake, Class. Quantum Grav. **13**, 1885 (1996)
27. E. Poisson, M. Visser, Phys. Rev. D **52**, 7318 (1995)
28. F.S.N. Lobo, P. Crawford, Class. Quantum Grav. **21**, 391 (2004)
29. E.F. Eiroa, G.E. Romero, Gen. Relativ. Gravit. **36**, 651 (2004)
30. K.A. Bronnikov, R.A. Konoplya, A. Zhidenko, Phys. Rev. D **86**, 024028 (2012)
31. M. Sharif, M. Azam, J. Phys. Soc. Jp. **81**, 124006 (2012)
32. J.P.S. Lemos, F.S.N. Lobo, Phys. Rev. D **69**, 104007 (2004)
33. M. Thibeault, C. Simeone, E.F. Eiroa, Gen. Relativ. Gravit. **38**, 1593 (2006)
34. F. Rahaman, M. Kalam, S. Chakraborty, Gen. Relativ. Gravit. **38**, 1687 (2006)
35. J.P.S. Lemos, F.S.N. Lobo, Phys. Rev. D **78**, 044030 (2008)
36. M.G. Richarte, C. Simeone, Phys. Rev. D **80**, 104033 (2009)
37. S.H. Mazharimousavi, M. Halilsoy, Z. Amirabi, Phys. Rev. D **89**, 084003 (2014)

38. M.R. Setare, A. Sepehri, J. High. Ener. Phys. **03**, 079 (2015)
39. M. Sharif, F. Javed, Eur. Phys. J. C **81**, 47 (2021); Ann. Phys. **416**, 168146 (2020)
40. M. Sharif, F. Javed, Int. J. Mod. Phys. D **29**, 2050007 (2020); Astron. Rep.353 (2021)
41. G. Mustafa, X. Gao, F. Javed, Fortschr. Phys. **2022**, 2200053 (2022)
42. M. Sharif, F. Javed, Chin. J. Phys. **77**, 804 (2022)
43. F. Javed, S. Sadiq, G. Mustafa, I. Husnain, Phys. Scr. **97**, 125010 (2022)
44. F. Javed, S. Mumtaz, G. Mustafa, I. Husnain, W.M. Liu, Euro. Phys. J. C **82**, 825 (2022)
45. F. Javed, Euro. Phys. J. C **83**, 513 (2023); Annal. Phys. **458**, 169464 (2023)
46. F. Javed, M.H. Alshehri, Annal. Phys. **464**, 169658 (2024)
47. F. Javed, J. Lin, Chinese J. Phys. **88**, 786–798 (2024)
48. G. Fatima et al., Chinese J. Phys. **90**, 864–876 (2024)
49. G. Mustafa, et al.: arXiv:2404.17904 (2024)
50. G. Mustafa et al., Phys. Dark Universe **45**, 101508 (2024)
51. Yong Liu et al., Euro. Phys. J. C **83**, 584 (2023)
52. E.F. Eiroa, C. Simeone, Phys. Rev. D **76**, 024021 (2007)
53. E.F. Eiroa, Phys. Rev. D **80**, 044033 (2009)
54. M. Sharif, M. Azam, J. Cosmol. Astropart. Phys. **04**, 023 (2013)
55. M. Sharif, M. Azam, Eur. Phys. J. C **73**, 2407 (2013)
56. V. Varela, Phys. Rev. D **92**, 044002 (2015)
57. A. Eid, Adv. Stud. Theo. Phys. **9**, 503 (2015)
58. M. Sharif, F. Javed, Gen. Relativ. Gravit. **48**, 158 (2016)
59. M. Sharif, F. Javed, Astrophys Space. Sci. **364**, 179 (2019)
60. M. Sharif, F. Javed, Phys. Scr. **96**, 055003 (2021)
61. Li. Xiang-Qian, et al., Phys. Rev. D **107**, 104055 (2023)
62. F. Javed, A. Waseem, B. Almutairi, Eur. Phys. J. C **83**, 811 (2023)
63. H. Zhang et al., Bardeen black hole surrounded by perfect fluid dark matter. Chinese Phys. C **455**, 055103 (2021)

Springer Nature or its licensor (e.g. a society or other partner) holds exclusive rights to this article under a publishing agreement with the author(s) or other rightsholder(s); author self-archiving of the accepted manuscript version of this article is solely governed by the terms of such publishing agreement and applicable law.